Nanoscale

Accepted Manuscript

This article can be cited before page numbers have been issued, to do this please use: M. Emperauger, E. KUREK, F. Semmer, K. Perronet, J. Daniel, M. Blanchard-Desce and F. Marquier, *Nanoscale*, 2025, DOI: 10.1039/D4NR03526G.

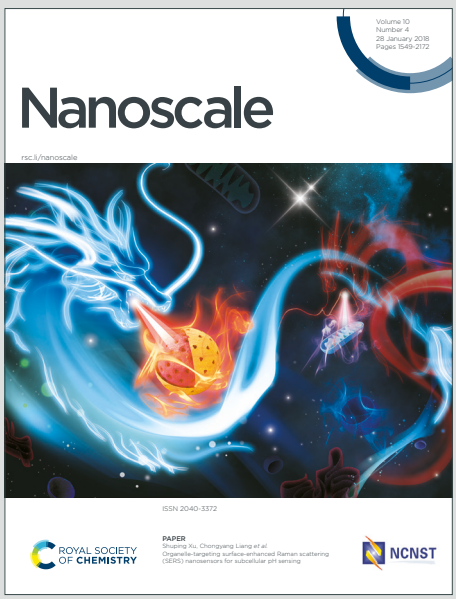

ROYAL SOCIETY OF CHEMISTRY

rsc.li/nanoscale

View Article Online
DOI: 10.1039/D4NR03526G

ARTICLE

3D Real-Time Single Particle Tracking using two-photon fluorescence from bright dye-based organic nanoparticles

Marie-Charlotte Emperauger†[a], Eleonore Kurek†[b], Florian Semmer[a]‡, Karen Perronet[a], Jonathan Daniel[b], Mireille Blanchard-Desce*[b], François Marquier*[a]

Received 00th January 20xx,
Accepted 00th January 20xx

DOI: 10.1039/x0xx00000x

This paper addresses the use of ultrabright dye-based fluorescent organic nanoparticles in a 3D single-particle tracking two-photon microscopy setup. The nanoparticles consist of an assembly of quadrupolar dyes, presenting a large two-photon absorption cross-section. They exhibit low photobleaching, crucial for long-term tracking, and their high brightness allows nanometer localization precision. Their small size compared to previously used nonlinear inorganic nanocrystals, stable structure at physiological temperature, and adjustable optical properties make them promising tools for further biological research. This study highlights their potential to track dynamic processes with precision and stability, paving the way for exploring cellular processes at the nanoscale.

Introduction

Single Particle Tracking (SPT) techniques enable exploration of biological dynamics at the molecular or cellular level. This includes for instance investigating biomolecule diffusion on membranes[1], or neuronal transport mechanisms[2], mediated by various families of molecular motors. The particles are tracked using their optical signal, which can be fluorescence, as in the case of molecules[3], quantum dots[4], NV centers in diamond nanocrystals[5,6], dye-based organic nanoparticles[7,8] or scattering, as in the case of gold nanoparticles[9]. SPT techniques require highly precise nanoparticle localization, about twenty nanometers at a rate of several tens of hertz for video-microscopy techniques[2,6], up to the recently achieved exceptional precision of 2 nm below millisecond temporal resolution with MINFLUX or MINSTED techniques[10,11]. This ultimate precision has enabled the observation of the fine mechanics of kinesin motors, even capturing the detachment moments of each motor head from the microtubule during steps[12]. However, rapid photobleaching of fluorescent molecules limits observations to a few hundred of milliseconds, drastically restricting the interrogation time. We recently developed a two-photon microscope, 3D-Red Shot, capable of real-time tracking (~700 Hz) of a nonlinear nanocrystal, through its second harmonic signal with a localization precision below 5 nm in the sample plane[13]. As second harmonic generation (SHG) is a coherent scattering process, we circumvent both photobleaching and blinking issues. Moreover, infrared excitation and nonlinear response offer two significant advantages: deeper penetration into biological tissues[14] and easy access to 3D observation through optical sectioning, as demonstrated, for example, when tracking nanocrystals in zebrafish larvae[15]. However, because achieving excellent localization precision is related to the number of photons received during a measurement, the nanocrystals must be large, with diameters around 120-150 nm for $BaTiO_3$ nanocrystals. Although larger diameters would lead to larger signals (in the case of SHG, the detected signal is proportional to the square of the nanoparticle volume), it is necessary to keep the nanoparticles much smaller than the wavelengths involved to maintain localization accuracy and not to interfere with biological processes. Ultimately, an ideal nano-probe should have a maximal signal level for a minimal size and without photobleaching nor blinking effects. Yet, smaller $BaTiO_3$ nanocrystals would lead to much smaller SHG signals (typically 10 times smaller for diameters of about 40-50 nm). In that perspective, nanoparticles showing large two-photon excited fluorescence (TPEF) would be an attractive alternative if photobleaching can be controlled. Having this goal in mind, we report the design of dye-based fluorescent organic nanoparticles (dFONs)[8], consisting of an assembly of dedicated quadrupolar dyes, 2 to 3 times smaller than the previously used $BaTiO_3$ nanocrystals, and demonstrate their successful use of 3D-Red Shot to track them. The present dFONs, hereafter named Nano2Track-840/650, were indeed shown to exhibit very large two-photon brightness[16,17], up to 10^6 GM, resulting in a nominal two-photon fluorescence level of about $0.5 - 1 \times 10^6$ photons/s detected from a single nanoparticle in the 3D-Red Shot setup. In comparison, the two-photon absorption cross-section of typical organic probes is around $10 - 100$ GM[18], while for 100 nm diameter $BaTiO_3$

[a] Université Paris-Saclay, École Normale Supérieure Paris-Saclay, CNRS, CentraleSupélec, LuMIn, 91190 Gif-sur-Yvette, France.
[b] Univ. Bordeaux, CNRS, Bordeaux INP, ISM (UMR5255), 351 Cours de la Libération, 33405 Talence, France.
† These authors contributed equally.
‡ Current address: Laboratoire Charles Fabry, Institut d'Optique Graduate School, CNRS, Université Paris-Saclay, 91127 Palaiseau, France.
*mireille.blanchard-desce@u-bordeaux.fr, francois.marquier@ens-paris-saclay.fr
Supplementary Information available: supporting figure on individual dyes and Nano2Track-840/650 nanoparticles. See DOI: 10.1039/x0xx00000x

nanocrystals, SHG scattering cross-sections have been reported between 1.4×10^3 and 2×10^3 GM[19]. Interestingly, by playing on the nature of the quadrupolar constituting dyes, dFONs combining large two-photon brightness and limited photobleaching[7], can be achieved, allowing SPT for tens of seconds when excitation is at saturation power. Additionally, the Nano2Track-840/650 dFONs structure remains stable at physiological temperatures and their photoluminescence is not altered at 37°C. These characteristics have allowed us to achieve ultimate localization precisions of around 3 nm and to track these nanoparticles in diffusion over distances of several tens of micrometers.

Results and discussion

Nano2Track-840/650 preparation, characterisation and stability

dFONs are a singular class of organic nanoparticles as they are made only of pure dedicated molecular dyes and can be easily prepared in water using green protocols. One of the main advantages of dFONs is that their optical (emission, brightness, nonlinear optical responses), their physicochemical properties (including colloidal, structural and photo- stabilities) and their nanobiointerface can all be bottom-up engineered by tuning the structure of specific dyes, i.e., polar and polarizable dyes[8,16,17]. Figure 1 summarizes the synthesis of Nano2Track-840/650 dFONs as well as their main fluorescence and two-photon absorption characteristics. Briefly, a non-water-soluble hydrophobic quadrupolar dye DyRed-510/650 is built from a fluorenyl core having two long alkyl pendent chains (in order to favor its solubility in THF) and bearing two strong electron-withdrawing end groups (Fig. 1a) which are responsible for its strong one- and two-photon absorption properties and red-shifted emission[16]. Nano2Track-840/650 nanoparticles are readily obtained using a nanoprecipitation process (Fig. 1a): upon addition of a minute amount of a stock solution of dyes DyRed-510/650 in THF to a large volume of distilled water, a red non-turbid solution is obtained. Transmission Electron Microscopy (TEM) observations show that the obtained nanoparticles are spherical (Fig. 1c). Analysis of the TEM images allows estimating the size distribution of Nano2Track-840/650 illustrated by the histogram in Fig. 1c. A broad size distribution is revealed: over half of the nanoparticles have small diameter (in between 10 and 30 nm) while bigger ones are also observed, having diameter in the 40-70 nm range (about 20 %) or even bigger in the 70-130 nm range (about 20 %). The resulting mean diameter of the nanoparticles is $\overline{D} \approx 46$ nm with a standard deviation of 30 nm. Dynamic Light Scattering (DLS) experiments are also performed in order to investigate both the Nano2Track-840/650 size distribution in water and their colloidal stability. They reveal an average hydrodynamic diameter of about 70 nm (Figure S1a and Table S1) with polydispersity index of 0.12. We attribute this larger average value to the DLS limitations, due in our case on the one hand to very low concentrations of nanoparticles (typically sub-nanomolar), and on the other to the very small difference in refractive index between water and dye-based materials. In fact, the present dFONs are designed to be used as bright nanoprobes for bioimaging and single particle tracking, thus very low concentrations are needed. In contrast, chemical, colloidal and photo-stabilities are mandatory to such applications. In that respect, DLS demonstrates that the nanoparticles show good colloidal stability: only a slight increase in size is observed after 10 weeks while larger sizes and partial setting is observed only after one year (see Figure S1a and Table S1). The high colloidal stability of the Nano2Track-840/650 suspension may be explained by the large negative zeta potential value (-52 mV) of the nanoparticle (Figure S1b). Fluorescence properties over time provide evidence of their chemical and structural stability (Figure S1c-d).

Nano2Track-840/650 visible absorption and photoluminescence properties

Nano2Track-840/650 strongly absorbs in the visible region and emits in the deep red region down to the beginning of the NIR. The absorption spectrum of Nano2Track-840/650 is broadened compared to individual dyes in solution (Figure S2a-b), with the full-width at half-maximum increasing from 96 nm to 132 nm (corresponding to 3400 and 5100 cm^{-1} respectively) and the maximum absorption shifting from 528 nm in toluene to 511 nm for Nano2Track-840/650 in water. The marked broadening of the absorption spectrum and the presence of shoulders at 475 nm (blueshifted) and 550 nm (redshifted) suggest excitonic coupling between dyes within Nano2Track-840/650, leading to Davydov splitting of the excited states. Consistently, the photoluminescence properties of Nano2Track-840/650 significantly differ from those of the individual dyes dissolved in an organic solvent (Figure S2c). In particular, the emission spectrum is altered, with the emission maximum shifting from $\lambda_{\mathrm{DyRed-510/650}}(\mathrm{toluene}) \approx 560$ nm to $\lambda_{\mathrm{Nano2Track-840/650}}\,(\mathrm{water}) \approx 650$ nm, thus extending to the beginning of the NIR1 region and increasing the Stokes shift, from 1100 cm^{-1} (33 nm) for DyRed-510/650 in toluene to 4200 cm^{-1} (142 nm) for Nano2Track-840/650 nanoparticles in water (Figure 2a) due to confinement effects (including excitonic coupling between dyes)[7,8].

Thanks to its quadrupolar nature,[16] DyRed-510/650 (in toluene) shows significant two-photon absorption (2PA) cross section (σ_2) in the NIR region, with maxima around 900 nm ($\sigma_2^{\max 1}$= 934 GM) and 800 nm ($\sigma_2^{\max 2}$= 1622 GM) (Figure S2d). Nano2Track-840 (in water) also shows significant broadband two-photon absorption in the near-infrared (NIR) with a peak around $\lambda \approx 840$ nm (Fig. 1d). Finally, as expected from molecular confinement effects, the 2PA spectrum of dyes within Nano2Track-840/650 differs from that of isolated dyes DyRed-510/650 (Figure S2d). A broadening of the 2PA response (including new sub-bands) is observed as well as an increase of the 2PA maximum cross-section now located at 840 nm ($\sigma_2^{\max}$= 1860 GM). Such effect of the molecular confinement on the 2PA response of quadrupolar dyes within dFONs was also reported earlier in dFONs made from different quadrupolar dyes[8,17]. Interestingly, thanks to these effects,

View Article Online
DOI: 10.1039/D4NR03526G

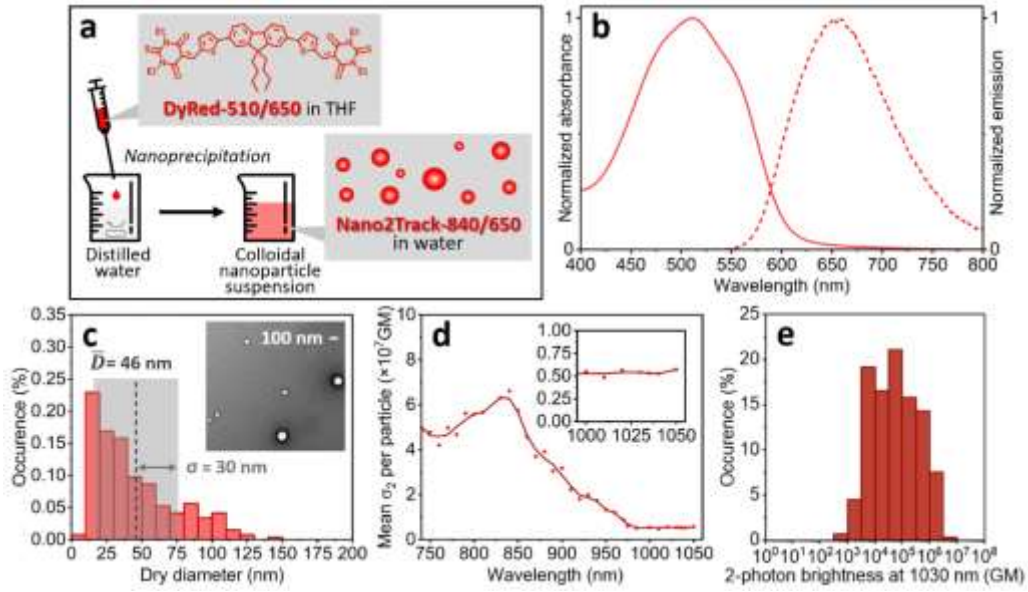

Figure 1. Properties of Nano2Track-840/650 nanoparticles. (a) Preparation scheme of Nano2Track-840/650 from DyRed-510/650 dye using nanoprecipitation. (b) Normalized absorption (solid) and emission (dashed line) spectra of Nano2Track-840/650 nanoparticles in water. (c) Size distribution of dry diameters of Nano2Track-840/650 obtained via transmission electron microscopy (TEM) on N=266 particles, with a mean value of $\bar{D} \approx 46$ nm, and a standard deviation of $\sigma \approx 30$ nm. Inset: representative TEM image. (d) Dots: Two-photon absorption cross-section $\sigma_2^{1\times \mathrm{Nano2Track-840/650}}$ of one average Nano2Track-840/650 nanoparticle, calculated as the product of the experimentally determined two-photon absorption cross-section $\sigma_2^{1\times \mathrm{DyRed-510/650}}$ of a single DyRed-510/650 molecule within Nano2Track-840/650 in water (Fig. S2d) and n, the number of DyRed-510/650 molecules in one 46 nm diameter nanoparticle (estimated at 3.5×10^4 molecules). Line: Mean fit. (e) Two-photon brightness distribution at 1030 nm for Nano2Track-840/650 nanoparticles of different diameters, calculated for each nanoparticle as the product of the experimentally determined two-photon absorption cross-section $\sigma_2^{1\times \mathrm{DyRed-510/650}}$ of a single DyRed-510/650 molecule within Nano2Track-840/650 in water (Fig. S2d), the fluorescence quantum yield of DyRed-510/650 within Nano2Track-840/650 and n, the number of DyRed-510/650 molecules per nanoparticle, calculated for each diameter of the size ditribution in figure 1c.

wavelength used for our tracking experiments (Figure S2c) and falls into the second transparency window of biological tissues (NIR2)[20]. At this wavelength, the two-photon absorption cross-section of Nano2Track-840/650 is still very high, around 5×10^6 GM (Fig. 1d). The two-photon emission cross-section (two-photon brightness) of a dFON is defined as the average product of the number of dyes making up the nanoparticle, the absorption cross-section of an individual dye molecule in this confined environment and its quantum fluorescence efficiency (2% for Nano2Track-840/650). Thus at $\lambda \approx 1030$ nm, the two-photon brightness (B_{2P}) of Nano2Track-840/650 ranges roughly from 10^4 to 10^6 GM depending strongly on the size of individual nanoparticles (Fig. 1e). More specifically, Nano2Track-840/650 nanoparticles of 46 nm in diameter exhibit B_{2P} values of 1.3 10^6 GM at 840 nm (maximum) and 1.1 10^5 GM at 1030 nm. These values compare well with the two-photon brightness values previously reported for dFONs having similar emission maxima and quantum yields[16,17,21]. It should be noted that molecular engineering of dipolar dyes as dFONs building block[8] may lead to even larger brightness at 1070 nm while further redshifting the emission[22], offering interesting promises for two-photon single particle tracking into biological tissues (i.e. excitation in the NIR2 and emission in the NIR1).

Two-photon single particle tracking of Nano2Track-840/650

Nano2Track-840/650 nanoparticles are observed in the two-photon SPT setup "3D-RedShot"[13], adapted to the fluorescence of the nanoparticles. Excitation (femtosecond laser, Chameleon ultra 2 Coherent, excitation wavelength: $\lambda_{exc} = 1028$ nm, pulse width 140 fs at 80 MHz) and fluorescence are separated by a dichroic mirror (FF749 Semrock), and the residual excitation laser is filtered before the photon counting module by two filters (FF01-842/SP25, and FF01-945/SP25, Semrock). The excitation laser is focused close to the diffraction limit (Gaussian distribution of its intensity with standard deviation of approximately 310 nm) by a high numerical aperture microscope objective (Nikon PlanApo VC, 60x, 1.2NA). We first characterize the two-photon fluorescence response of a panel of individual nanoparticles fixed on a glass coverslip (see methods). Figure 2a presents the fluorescence photon counting rate as a function of the excitation power. As expected for two-photon excited fluorescence, the dependence of the photon counting rate on the excitation power is quadratic for low power values (see Fig. 2a, inset). Saturation occurs at higher excitation powers. A simple model of emission yields a detected intensity:

$$I_{\mathrm{detected}} = \frac{I_0}{1 + \left(\frac{P_{sat}}{P_{exc}}\right)^2}$$

where P_{exc} is the excitation power, P_{sat} is the characteristic excitation power of fluorescence saturation, and I_0 is a fit parameter that depends in particular on the number of dye molecules into the observed nanoparticle and the overall collection efficiency of the system. From experimental data, we obtain $P_{sat} \approx 4.9$ mW (average power) in our system, corresponding to an average excitation intensity $I_{sat} \approx 0.8\ \mathrm{MW.cm^{-2}}$.

View Article Online
DOI: 10.1039/D4NR03526G

ARTICLE

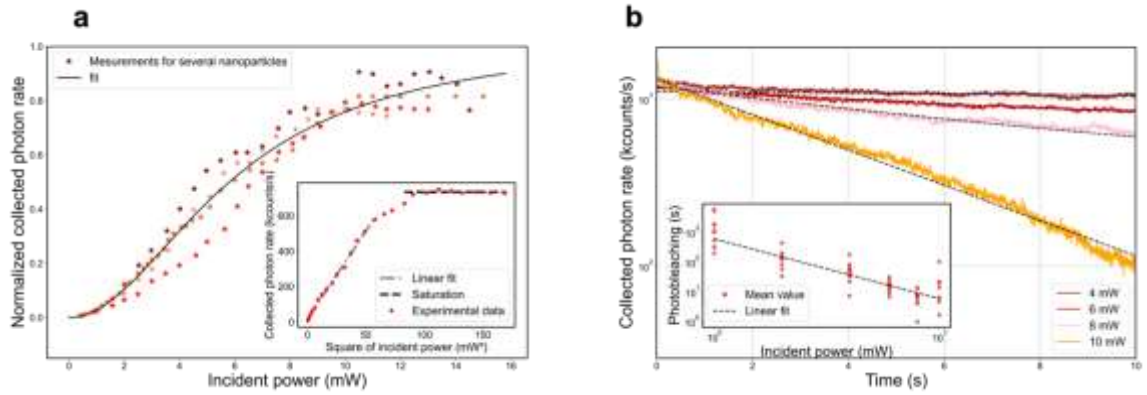

Figure 2. Saturation behavior of the two-photon fluorescence. (a) Normalized collected photon rate for several nanoparticles (in different colors) evolution with incident power and fit as in eq. (1) (black line) with $P_{sat} = 4.9$ mW and $I_0 = 9.3 \times 10^{-3}$ W/cm^2 as parameters. Inset: Collected photon rate for a given single nanoparticle as a function of incident power squared. Dotted lines correspond to two main behaviors: a quadratic dependence of photon counting rate on excitation power is observed at low power and saturation at high power. (b) Collected photon rate in log scale evolving with time for several nanoparticles illuminated at different incident powers. Black dotted lines are adjustments of the curves with a linear fit. Inset: Evolution of the photobleaching time τ_b of the collected photon rate of several nanoparticles at different incident powers. The black dotted line is a linear fit with a slope -2.

Figure 2b shows that the nanoparticles experience photobleaching with $1/e$ characteristic times τ_b up to several hundred seconds. τ_b quadratically depends on the inverse of the excitation power[23], i.e. the absorption rate. First, it indicates that no obvious higher-order nonlinear processes are involved in the photobleaching of dFONs, unlike what has been observed for some individual dye molecules[24,25]. Second, it points out that τ_b is inversely proportional to the absorption cross-section. We should thus expect much shorter characteristic bleaching times τ_b (one order of magnitude below) at $\lambda_{exc} \approx 840$ nm, corresponding to the maximum of the two-photon absorption cross-section. Consequently, being above $\lambda_{exc} > 1000$ nm appears as a fair trade-off between a lower (but still large) brightness and a higher photostability compared to an excitation at $\lambda_{exc} \approx 840$ nm. The photon rates collected for several nanoparticles and at various excitation powers (inset of Figure 2b) are fitted by a power law $\tau_b = \tau_{b0} \left(\frac{P_{sat}}{P}\right)^2$ (dotted lines) with a parameter $\tau_{b0} \approx 24$ s. This characteristic photobleaching time is of the same order of magnitude as those observed for other dFONs [7,8], and several orders of magnitude above the characteristic times of most individual dye molecules upon two-photon excitation (on the order of a few tens of µs at saturation)[25]. In most experiments, we choose an excitation power $P = \frac{P_{sat}}{5} \approx 1$ mW, leading to τ_b of several minutes. The remarkable photostability and brightness of Nano2Track-840/650 suggest they could be well-suited for super-localization SPT experiments.

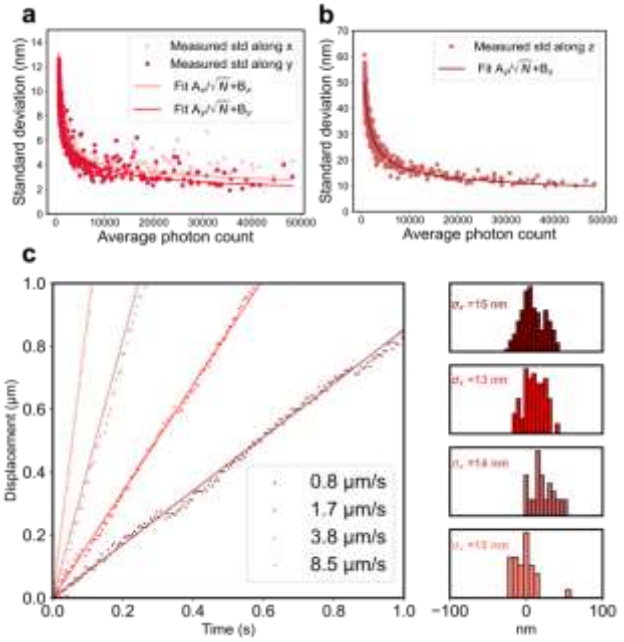

Figure 3. Localization precision of fixed Nano2Track-840/650 nanoparticles in the plane orthogonal to the optical axis (a) and along the optical axis (b). In both experiments, incident power is 4 mW. Experimental data are fitted with a B+A/$\sqrt{N}$ law. Fit parameters: $A_x = 218$ *et* $B_x = 1.8$ nm, $A_y = 236$ *et* $B_y = 1.2$ nm, $A_z = 1159$ *et* $B_z = 4.7$ nm (c) Left: tracks of a nanoparticle moved by a piezo stage at different velocities. The dots stand for the measured displacements and the plain lines for the piezo-stage programmed motions. The incident power is 1 mW. (c) Right: histograms of the errors to the piezo-stage positions. The indicated localization precisions σ_x of the moving particle are estimated by standard deviations of the distributions of errors. The standard deviations are around 15 nm for all

tested velocities and correspond to the expected values at the average number of collected photons from the tracked single nanoparticle.

The 3D-RedShot setup relies on a two-photon SPT method in which a nanoemitter is tracked in 3D using an excitation laser focused near the emitter following a predetermined spatial sequence controlled by a digital micromirror device (DMD). The signal, collected by a photon counting module, depends on the distance between the emitter and the focal point of the excitation laser. It is thus possible to deduce the emitter's position with very high precision using a maximum likelihood estimation[11]. The localization precision of the system for this type of nanoemitter can be obtained by repeating SPT measurements on a fixed particle and calculating the standard deviation of the measured positions. When exciting a single nanoparticle, the number of collected photons N decreases due to photobleaching, so that it is possible to verify on Figures 3a and 3b that the achieved precisions vary as $1/\sqrt{N}$. A fit of the data gives an ultimate precision around 2 nm in the plane orthogonal to the optical axis (x and y directions) and 5 nm along the axis (z). More reasonably, we achieve localization precisions of 3 nm and 10 nm respectively for a total number of received photons of 2×10^4, corresponding to long integration times of a few hundreds of ms depending on the nanoparticle size.

In a dynamic tracking experiment, the integration time to get a single position is much shorter, from 2 to 10 ms, resulting in slightly lower localization precision. To assess position uncertainties when the particle is in motion, we move the nanoparticle using a piezoelectric stage in a uniform linear motion at different speeds. The results are summarized in Figure 3c. It is observed that it is possible to track Nano2Track-840/650 nanoparticles at relatively high speeds while maintaining very good localization precision on the order of 15 nm in the (x, y) plane. This result is in agreement and comparable to previously obtained results[13] with inorganic nanocrystals of $BaTiO_3$ whose typical diameters were 2 to 3 times larger.

Nano2Track-840/650 nanoparticles are then tracked for several minutes while diffusing in a glycerol-water mixture (64% w/w) with an estimated viscosity of 13 mPa.s. Figure 4a shows an example of a nanoparticle diffusion trajectory. The collected photon rate is stable over time (Fig. 4b) shows that the particle undergoes almost no photobleaching throughout the duration of the measurement (4 min). Plotting all data points as a function of time allows us to construct the three-dimensional Mean Squared Displacement (MSD) as a function of time delay Δt between pairs of points (Fig. 4c). Purely diffusive behaviour is characterized by a linear dependence $\mathrm{MSD}(\Delta t) = 6D_{\mathrm{diff}}\Delta t$ where D_{diff} is the diffusion coefficient of the nanoparticle in the medium. The slope given by the first two points of the MSD contains the optimal level of information for a linear fit of the data and thus an estimation of D_{diff}[26]. The Stokes-Einstein relation for a spherical particle then allows us to calculate the nanoparticle radius. Consequently, we are able to measure the diameters of 50 different particles in solution. The result presented in Fig. 4d shows excellent agreement with the diameter measurements obtained by TEM microscopy.

In a final experiment, we observe the diffusion of Nano2Track-840/650 nanoparticles in a $400\ \mathrm{mg.mL^{-1}}$ solution of bovine serum albumin (BSA) maintained at a temperature of 37°C. The viscosity of the solution at this temperature is lower than in the previous experiments in the glycerol-water mixture, on the order of 9 mPa.s. Figure 4e displays an example of nanoparticle diffusion under these conditions. The collected photon rate measured over a 6-minute duration presented in Figure 4f shows that the signal remains perfectly stable over time. Thus, Nano2Track-840/650 nanoparticles are not only photostable (experiencing low photobleaching) but also structurally stable under biological conditions (in the presence of various bioorganic molecules and at physiological temperatures). These results highlight the strong potential of Nano2Track-840/650 for uses in SPT experiments to track biological processes, akin to other nanoprobes such as inorganic nanocrystals[4,5,13]. In that respect, we stress that such type of dFONs can be further surface-functionalized by building a shell of dedicated dyes that can undergo click functionalization in water[27].

View Article Online
DOI: 10.1039/D4NR03526G

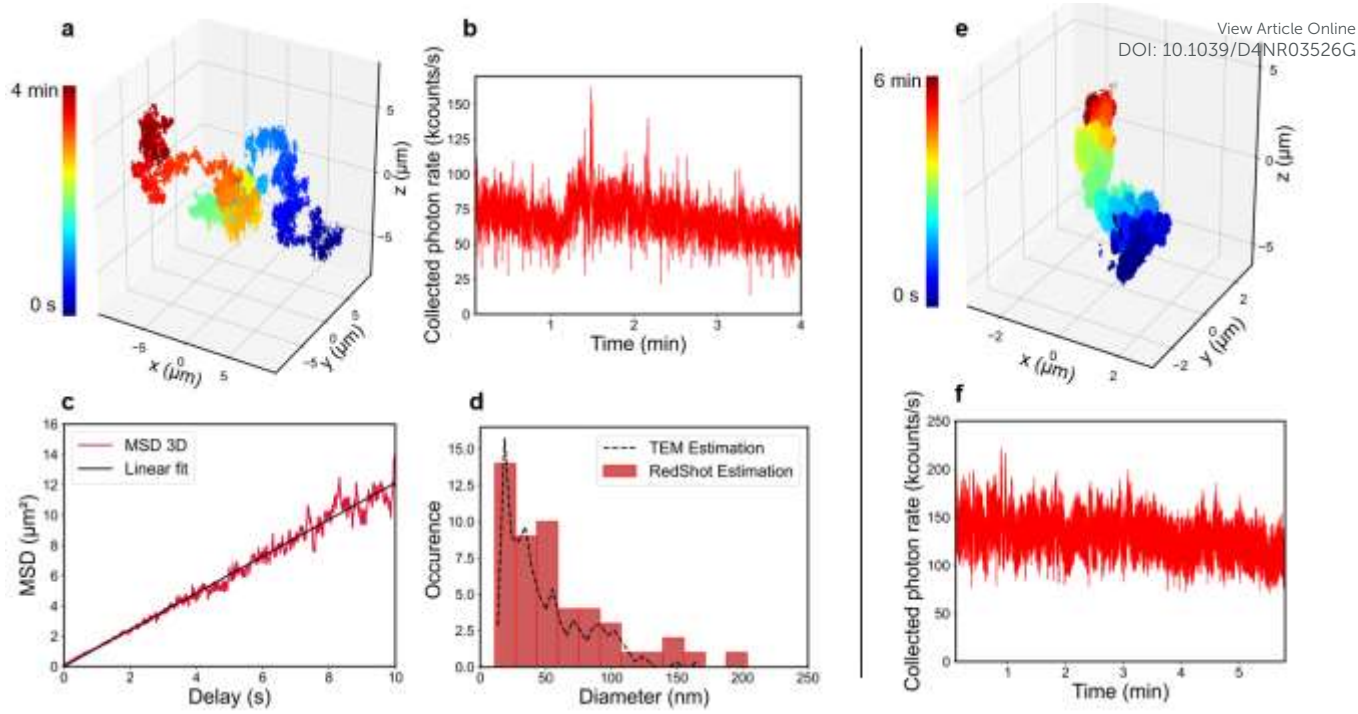

Figure 4. Tracking of freely moving particles. (a) 3D Trajectory of a single freely moving particle in a water/glycerol mixture (64% w/w) at a localization rate of 93 Hz. The color code corresponds to the time, from blue at the beginning of the trajectory to red at the end. The duration of the displayed trajectory is 4 min. (b) Detected counts from the fluorescence signal during the measurement, we verified that the increase of intensity observed just after 1 min is due to a significant change in the z position (from ≈ -5 µm to ≈ 1 µm in the blue-color section of the trajectory on Fig 4(a)). Indeed, the particle does not experience the same exact excitation intensities when moving into the excitation pattern, particularly along the z direction, as less points of the pattern are associated to the z localization. (c) Mean Square Displacement (MSD) in 3 dimensions versus lag time. (d) Comparison of the NC size measured from the diffusion coefficient for several trajectories (red bars) and the size distribution measured by TEM (black dot curve). (e) 3D Trajectory of a single freely moving particle in a water/BSA mixture (concentration of 400 mg. mL^{-1}) at a localization rate of 713 Hz. The colour code corresponds to the time, from blue at the beginning of the trajectory to red at the end. The duration of the displayed trajectory is 6 min. (f) Detected counts from the fluorescence signal during the measurement. All experiments are performed with 1 mW incident power.

Conclusions

We have demonstrated the possibility of using dye-based fluorescent organic nanoparticles in two-photon single-particle tracking experiments. Their exceptionally high brightness allows for precise position estimation in a super-localization regime, their photobleaching is particularly slow (several tens of seconds at saturation), and their structure is stable at physiological temperatures. These properties make them potentially compatible with biological applications, pending validation of their non-toxicity. It is worth noting that for organic nanoparticles, the fluorescence intensity will always be limited by saturation at higher excitation powers, whereas for nanocrystals, second harmonic generation will continue to increase with the square of the excitation power. However, the two-photon brightness cross-section of Nano2Track-840/650 is much larger (4 orders of magnitude) than the two-photon scattering cross-section (SHG efficiency) of $BaTiO_3$ nanocrystals[13,19] brought to the same typical size (around 10 GM for a 46 nm diameter nanocrystal and 2×10^3 GM for a 100 nm diameter). In other terms, these dFONs will be brighter than the nanocrystals at low excitation power. Moreover, when excited below the saturation, the characteristic times before photobleaching of Nano2Track-840/650 can be substantial, granting up to several minutes with sufficient signal to allow for long-term tracking in SPT. In this low power regime, which may be needed to minimize photo-induced damages in sensitive samples, organic dFONs such as Nano2Track-840/650 are therefore much more advantageous than nanocrystals. In addition, such dFONs could be surface-functionalized with targeting or binding moieties, which paves the way to real-time single-particle tracking of membrane receptors, or molecular motors for instance.

Experimental methods

Nanoparticles preparation

The synthetic scheme of DyRed-510/650 is described in Figure S2e.

Synthesis of A (dye precursor). Air was removed from a solution of 2,7-diiodo-9,9-dibutyl-9H-fluorene[28] (0.15 g, 0.3 mmol) and 5-formyl-2-thienylboronic acid (0.18 g, 1.1 mmol) in toluene/methanol (2:1, 9 mL) in which potassium carbonate (0.42 g, 3.0 mmol) and [$PdCl_2$(dppf)] (4 mg, 5.5 µmol) had been added by blowing argon for 15 min. The suspension was then stirred and heated to reflux for 3 days. Thereafter, solvents were evaporated under reduced pressure then the dark residue was dissolved in dichloromethane and the

resulting reddish solution was washed three times with water. After drying over Na_2SO_4, the organic layer was filtered, concentrated and finally purified by chromatography (petroleum ether/dichloromethane, 1:4). The fractions containing A were gathered and solvents were removed under reduced pressure to yield 82 mg (53%) of pure A as a yellow powder.

Characterization of A. Proton (^{1}H) NMR (300 MHz, $CDCl_3$): $\boldsymbol{\delta}$ = 9.93 (s, 2H), 7.80 (d, *J*= 3.9 Hz, 2H), 7.78 (d, *J*= 0.5 Hz, 2H), 7.72 (dd, *J*= 7.8 Hz, *J*= 1.6 Hz, 2H), 7.66 (dd, *J*= 1.6 Hz, *J*= 0.5 Hz, 2H), 7.52 (d, *J*= 3.9 Hz, 2H), 2.07 (m, 4H), 1.14 (m, 4H), 0.70 (t, *J*= 7.2 Hz, 6H), 0.65 (m, 4H). Carbon-13 (^{13}C) NMR (150 MHz, $CDCl_3$): 182.7, 154.8, 152.2, 142.2, 141.6, 137.4, 132.4, 125.7, 124.0, 120.8, 120.7, 55.5, 40.1, 26.0, 23.0, 13.8. High-resolution mass spectrometry (HRMS): $C_{31}H_{31}O_2S_2$ theoretical $[M\text{-}H]^+$= 499.17600, measured $[M\text{-}H]^+$= 499.17586.

Synthesis of DyRed-510/650. In a 25 mL round flask, a solution of A. (50 mg, 0.1 mmol), 1,3-diethyl-2-thiobarbituric acid (48 mg, 0.24 mmol) and catalytic amount of $\boldsymbol{\beta}$-alanine in absolute ethanol (3.0 mL) was refluxed for 24h. The mixture was left to cool down to room temperature and the red dark precipitate was filtrated, then washed with absolute ethanol. The powder was then dried under reduced pressure to yield 33 mg (38%) of pure DyRed-510/650.

Characterization of DyRed-510/650. Proton (^{1}H) NMR (300 MHz, $CDCl_3$): $\boldsymbol{\delta}$ = 8.72 (s, 2H), 7.95 (d, *J*= 4.4 Hz, 2H), 7.88 (dd, *J*= 8.0 Hz, *J*= 1.5 Hz, 2H), 7.82 (d, *J*= 8.0 Hz, 2H), 7.79 (d, *J*= 1.2 Hz, 2H), 7.66 (d, *J*= 4.2 Hz, 2H), 4.67 (Q, *J*= 7.0 Hz, 4H), 4.62 (Q, *J*= 7.0 Hz, 4H), 2.14 (m, 4H), 1.41 (t, *J*= 7.0 Hz, 6H), 1.36 (t, *J*= 7.0 Hz, 6H), 1.14 (m, 4H), 0.70 (t, *J*= 7.2 Hz, 6H), 0.65 (m, 4H). Carbon-13 (^{13}C) NMR (75 MHz, $CDCl_3$): 178.7, 161.9, 161.0, 160.0, 152.4, 149.6, 147.5, 142.3, 136.8, 132.7, 126.4, 125.1, 121.0, 120.9, 110.2, 55.8, 44.0, 43.2, 40.2, 26.0, 23.0, 13.8, 12.6, 12.4 ppm. High-resolution mass spectrometry (HRMS): $C_{47}H_{51}O_4N_4S_4$ theoretical $[M\text{-}H]^+$= 863.27877, measured $[M\text{-}H]^+$= 863.27992.

Preparation of the Nano2Track-840/650 nanoparticles. A stock solution of DyRed-510/650 (4 mM in THF) was added dropwise into freshly distilled water (1% v/v) under magnetic stirring (900 rpm, 30 min). The solution was then centrifuged at 3000 rpm for 5 minutes.

Photo-physical characterisation. Absorbance measurements were performed at room temperature using a Jasco V-670 UV/Vis spectrophotometer. Emission spectra were acquired using a FluoroMax spectrofluorometer, on diluted solutions with an absorbance maximum set to ≤ 0.1. All measurements were made in 1 cm quartz cuvettes, on freshly prepared DyRed-510/650 molecular solutions in toluene or Nano2Track-840/650 nanoparticles in water. Fluorescence quantum yields Φ_f were measured relative to 4-Dicyanomethylene (DCM) in ethanol using the following formula:

$$\Phi_f = \frac{n^2}{n_{DCM}^2} \times \frac{\int I_F}{\int I_{F\,DCM}} \times \left(\frac{1-10^{-A_{DCM}}}{1-10^{-A}}\right) \times \Phi_{DCM} \text{szqQ} \quad \text{Q}$$

Φ_{DCM} is the fluorescence quantum yield of the standard DCM (Φ_{DCM} = 0.44 in EtOH), $\int I_F$ is the area under the curve of the emission spectrum of the sample excited at λ_{ex}, , $\int I_{F\,DCM}$ is the area under the curve of the emission spectrum of the reference DCM excited at $\lambda_{ex\ DCM}$, A is the absorbance of the sample at λ_{ex}, A_{DCM} is the absorbance of DCM at $\lambda_{ex\ DCM}$, n is the refractive index of the sample solvent and n_{DCM} is the refractive index of the reference solvent (Φ_{EtOH} = 1.361). The sample and standard measurements were taken with the same experimental parameters: on the same day, with the same spectrometers, cuvettes and slits.

Two-photon absorption cross section measurements.

Two-photon absorption cross-sections ($\boldsymbol{\sigma_2}$) were determined from the two-photon brightness ($\boldsymbol{\sigma_2\Phi}$) measured using the Two-Photon Excited Fluorescence technique (TPEF)[29]. TPEF measurements were performed on molecular solutions of DyRed-510/650 in toluene ($\boldsymbol{4.0 \times 10^{-5}\ M}$) and Nano2Track-840/650 nanoparticles in water ($\boldsymbol{2.9 \times 10^{-5}\ M}$). A Ti:Sapphire oscillator (Coherent Chameleon Ultra II, Nd:YVO4, 140 fs, 80 MHz) was tuned from 700 nm to 1050 nm and focused onto the sample through a 10X achromatic objective (Olympus PN, NA 0.25). Fluorescence emission was collected at 90° using a 10x achromatic objective (Olympus UPFLN, NA 0.30) and sent on a compact USB CCD spectrometer (Maya2000Pro Ocean Insight) through an optical fiber. Responses were measured against Fluorescein ($\boldsymbol{1.16 \times 10^{-4}\ M}$ and $\boldsymbol{1.3 \times 10^{-5}\ M}$) in NaOH 0.01 M, as well as Nile Red in DMSO ($\boldsymbol{1.00 \times 10^{-4}\ M}$). For each solvent, the appropriate refractive index corrections were made. The quadratic dependence of the fluorescence intensity on the excitation power was checked at all wavelengths. More details about the homemade software used can be found on github (https://github.com/LAGONteam/PyTwoPhotonExcitedFluorescence).

Transmission Electron Microscopy.

Transmission Electron Microscopy was performed on a Hitachi H7650 electron microscope. Copper grids coated with a polymer membrane were positively ionized. A drop of undiluted dFONs solution was deposited on the grids for 1 minute, then the excess was removed using paper. Uranyl-acetate was deposited using the same procedure for 3 minutes. Size analysis was conducted on the obtained images by hand, using ImageJ software. The average number of dye subunits per particle was calculated using the resulting radius values, assuming the particles were of spherical shape with a density of 1.

Dynamic Light Scattering and zeta potential

Hydrodynamic diameters were determined by Dynamic Light Scattering (DLS) on a Zetasizer Nano SZ100Z Horiba instrument operating at 90°. Analysis was performed using the software supplied by the manufacturer, with a polydisperse and standard width size distribution as calculation settings. Diameters reported in Table S1 are the total mean values of number-based size distributions. Zeta-potential measurements and analyses were performed on the same SZ-100Z Horiba instrument.

Preparation of coverslips.

For localization precision experiments, a drop of solution (20µL) containing nanoparticles was deposited on a glass

coverslip. The coverslip was placed on a hot plate to accelerate the evaporation of water at 40°C during 15min.

Author contributions

MCE and EK performed the experiments under supervision of FM and KP, EK synthesized and characterized the dFONs under supervision of JD and MBD, FS and MCE built the two-photon microscope under supervision of FM and KP. FM and MBD are at the origin of this project. The manuscript was written through contributions of all authors. All authors have given approval to the final version of the manuscript.

Conflicts of interest

There are no conflicts to declare.

Data availability

The data that support the findings of this study are openly available on Zenodo, reference number 13382781, at https://doi.org/10.5281/zenodo.13382781.

Acknowledgements

This work has received financial support from the French National Research Agency ANR (ANR-18-CE09-0027), and from a public grant overseen by the ANR as part of the "Investissements d'Avenir" Program (reference: ANR-10-LABX-0035, Labex NanoSaclay). The research was supported by two Ph.D. scholarships, from ENS Paris-Saclay (MCE) and the University of Bordeaux (EK). The authors also acknowledge the support from the LIGHT S&T Graduate Program of Bordeaux (PIA3 Investment for the Future Program, ANR-17-EURE-0027). This work was partially supported by the European Commission. We thank Rosalie Tabarie for fruitful interactions concerning experimental data.

Notes and references

1 Y. Lee, C. Phelps, T. Huang, B. Mostofian, L. Wu, Y. Zhang, K. Tao, Y. H. Chang, P. J. S. Stork, J. W. Gray, D. M. Zuckerman and X. Nan, *Elife*, 2019, **8**, 1–23.

2 L. Kaplan, A. Ierokomos, P. Chowdary, Z. Bryant and B. Cui, *Sci Adv*, 2018, **4**, e1602170.

3 F. Wehnekamp, G. Plucińska, R. Thong, T. Misgeld and D. C. Lamb, *Elife*, 2019, **8**, 1–22.

4 B. Cui, C. Wu, L. Chen, A. Ramirez, E. L. Bearer, W. P. Li, W. C. Mobley and S. Chu, *Proc Natl Acad Sci U S A*, 2007, **104**, 13666–13671.

5 S. Haziza, N. Mohan, Y. Loe-Mie, A.-M. Lepagnol-Bestel, S. Massou, M. Adam, X. L. Le, J. Viard, C. Plancon, R. Daudin, P. Koebel, E. Dorard, C. Rose, F. Hsieh, C. Wu, B. Potier, Y. Herault, C. Sala, A. Corvin, B. Allinquant, H. Chang, F. Treussart and M. Simonneau, *Nat Nanotechnol*, 2017, **12**, 322–328.

6 Q.-L. Chou, A. Alik, F. Marquier, R. Melki, F. Treussart and M. Simonneau, *eNeuro*, 2022, **9**, ENEURO.0227-21.2022.

7 J. Daniel, A. G. Godin, M. Palayret, B. Lounis, L. Cognet and M. Blanchard-Desce, *J Phys D Appl Phys*, 2016, **49**, 084002. View Article Online DOI: 10.1039/D4NR03526G

8 J. Daniel, O. Dal Pra, E. Kurek, C. Grazon and M. Blanchard-Desce, *Comptes Rendus. Chimie*, 2024, **27**, 1–17.

9 A. R. Dunn and J. A. Spudich, *Nat Struct Mol Biol*, 2007, **14**, 246–248.

10 L. Scheiderer, H. von der Emde, M. Hesselink, M. Weber and S. W. Hell, *Nat Methods*, 2024, **21**, 569–573.

11 F. Balzarotti, Y. Eilers, K. C. Gwosch, A. H. Gynnå, V. Westphal, F. D. Stefani, J. Elf and S. W. Hell, *Science*, 2017, **355**, 606–612.

12 J. O. Wolff, L. Scheiderer, T. Engelhardt, J. Engelhardt, J. Matthias and S. W. Hell, *Science (1979)*, 2023, **379**, 1004–1010.

13 F. Semmer, M.-C. Emperauger, C. Lopez, C. Bogicevic, F. Treussart, K. Perronet and F. Marquier, *ACS Photonics*, 2023, **10**, 3426–3434.

14 K. Svoboda and R. Yasuda, *Neuron*, 2006, **50**, 823–839.

15 B. Grimaud, M. Frétaud, F. Terras, A. Bénassy, K. Duroure, V. Bercier, G. Trippé-Allard, R. Mohammedi, T. Gacoin, F. Del Bene, F. Marquier, C. Langevin and F. Treussart, *ACS Nano*, 2022, **16**, 20470–20487.

16 J. Daniel, A. G. Godin, G. Clermont, B. Lounis, L. Cognet and M. Blanchard-Desce, in *International Conference on Nano-Bio Sensing, Imaging, and Spectroscopy 2015*, 2015, vol. 9523.

17 P. Pagano, M. Rosendale, J. Daniel, J. B. Verlhac and M. Blanchard-Desce, *Journal of Physical Chemistry C*, 2021, **125**, 25695–25705.

18 J. Mütze, V. Iyer, J. J. Macklin, J. Colonell, B. Karsh, Z. Petrášek, P. Schwille, L. L. Looger, L. D. Lavis and T. D. Harris, *Biophys J*, 2012, **102**, 934–944.

19 Y. Pu, R. Grange, C. L. Hsieh and D. Psaltis, *Phys Rev Lett*, 2010, **104**, 207402.

20 S. Golovynskyi, I. Golovynska, L. I. Stepanova, O. I. Datsenko, L. Liu, J. Qu and T. Y. Ohulchanskyy, *J Biophotonics*, 2018, **11**, e201800141.

21 J.-B. Verlhac, J. Daniel, P. Pagano, G. Clermont and M. Blanchard-Desce, *Comptes Rendus. Chimie*, 2016, **19**, 28–38.

22 C. Mastrodonato, P. Pagano, J. Daniel, M. Vaultier and M. Blanchard-Desce, *Molecules*, 2016, **21**, 1227.

23 S. Gavrilyuk, S. Polyutov, P. C. Jha, Z. Rinkevicius, H. Ågren and F. Gel'mukhanov, *J Phys Chem A*, 2007, **111**, 11961–11975.

24 P. Yao, C. Van Vlack, a. Reza, M. Patterson, M. Dignam and S. Hughes, *Phys Rev B*, 2009, **80**, 195106.

25 P. S. Dittrich and P. Schwille, *Applied Physics B*, 2001, **73**, 829–837.

26 X. Michalet, *Phys Rev E*, 2010, **82**, 041914.

27 O. Dal Pra, J. Daniel, G. Recher, M. Blanchard-Desce and C. Grazon, *Small Methods*, DOI:10.1002/smtd.202400716.

28 J. Daniel, C. Mastrodonato, A. Sourdon, G. Clermont, J.-M. Vabre, B. Goudeau, H. Voldoire, S. Arbault, O. Mongin and M. Blanchard-Desce, *Chemical Communications*, 2015, **51**, 15245–15248.

29 C. Xu and W. W. Webb, *Journal of the Optical Society of America B*, 1996, **13**, 481.

The data that support the findings of this study are openly available on Zenodo, reference number 13382781, at https://doi.org/10.5281/zenodo.13382781.

View Article Online
DOI: 10.1039/D4NR03526G